SIMULATION OF DOUBLY FED INDUCTION GENERATOR WITH DIRECT POWER CONTROL

A PROJECT REPORT

Submitted in partial fulfillment of the requirements
For the award of the degree of

BACHELOR OF TECHNOLOGY

IN

ELECTRICAL ENGINEERING

By

HARIPRASAD R

(EE11B019)

Under the guidance of

Dr. KALYAN KUMAR B

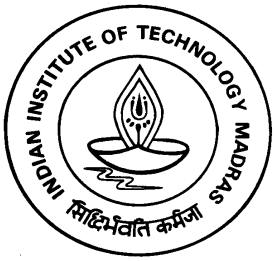

DEPARTMENT OF ELECTRICAL ENGINEERING

INDIAN INSTITUTE OF TECHNOLOGY, MADRAS

MAY 2015

ACKNOWLEDGEMENT

I would like to express my sincere thanks to my guide **Dr. Kalyan Kumar B** for his guidance with suggestions and discussions at various stages throughout my project work. He took out his valuable time for me from his rigorous schedule as an associate professor in order to clarify various doubts that I posed from time to time. I got a very good picture of Electrical Machines from this project all due to his direction.

Hariprasad R

EE11B019

CERTIFICATE

This is to certify that the project report entitled **"*SIMULATION OF DOUBLY FED INDUCTION GENERATOR WITH DIRECT POWER CONTROL*"** submitted by Hariprasad R (EE11B019) to the Indian Institute of Technology Madras for the award of the degree of **Bachelor of Technology in Electrical Engineering** is an authentic record of project work carried out by him under my supervision. The contents of this report, in full or in parts, have not been submitted to any other Institute or University for the award of any degree or diploma.

Dr. Kalyan Kumar B
Associate Professor
Department of Electrical Engineering
Indian Institute of Technology Madras
Chennai – 600 036

ABSTRACT

Doubly fed induction generator (DFIG) is one practical means of harnessing wind energy for electrical power. This project is an attempt to study the principle of DFIG and its working which includes working of the Doubly fed induction machine (DFIM), working of the 2-level voltage source converter, grid-side control and rotor side control. Initially the rotor-side and the grid-side converters, grid-side control is explained. Grid-side control is achieved through Grid voltage vector oriented vector control (GVOVC) .Then the dynamic electrical model of the DFIM is explained. This is followed by the rotor-side control. In this project, rotor-side control is executed in Direct Power Control schema. Along with the theory, simulation diagrams for the above mentioned aspects of DFIG are developed. Employing them, the behavior of DFIG is recorded in response to certain stimuli such that the efficacy of the control mechanisms can be examined. These responses are then discussed and conclusions pertaining to control of DFIG are drawn.

LIST OF FIGURES AND TABLES

NOMENCLATURE AND ACRONYMS

DFIG- Doubly fed induction generator

DFIM- Doubly fed induction machine

[Note: In the entire report, DFIM represents a section of DFIG as shown in Fig 2.1 and not Doubly fed induction machines as given in the general literature, which represent both Doubly fed induction generator and Doubly fed induction motor]

DPC- Direct power control

VSC- Voltage source converter

GSC- Grid side converter

VSC- Voltage side converter

L_f- Inductance of the grid side filter

R_f- Resistance of the grid side filter

v_{ag} , v_{bg}, v_{cg}- Grid voltages with ω_s electrical angular speed

i_{ag} , i_{bg}, i_{cg}- Currents flowing through the grid side converter's output

v_{af} , v_{bf}, v_{cf}- Output voltages of the converter referred to the neutral point of the load

i_{res}- Current through the resistance

i_{g_dc}- DC current flowing from the DC link to the grid

i_{r_dc}- DC current flowing from the rotor to the DC link

v_a^*, v_b^*, v_c^*- Reference voltages for each phase

v_{tri}- Triangular signal

ω_r- Angular frequency of currents and voltage of the rotor windings

ω_s- Angular frequency of currents and voltage of the stator windings

ω_m- Angular frequency of rotor

Ω_m- Mechanical rotational speed

p- Number of poles

s- Slip

P_s- Stator active power

P_r- Rotor active power

P_{mech}- Mechanical power, power transmitted through the electrical circuit to the shaft

T_{em}- Electromagnetic torque in the shaft of the machine

T_{load}- Torque due to mechanical load on shaft of the machine

Q_s- Stator reactive power

Q_r- Rotor reactive power

u- u factor

$L_{\sigma r}$- Rotor leakage impedance

$L_{\sigma s}$- Stator leakage impedance

L_m- Magnetizing inductance of the machine

L_r- Rotor inductance

L_s- Stator inductance

R_r- Rotor resistance

R_s- Stator resistance

δ- Angle between stator flux and rotor flux space vector

$\sigma = 1 - \frac{L_m^2}{L_s L_r}$ is the Leakage coefficient

ψ_s- Stator flux

ψ_r- Rotor flux

CONTENTS

CHAPTER-1 INTRODUCTION

1.1 General Introduction

Wind power is an abundant, renewable, clean resource. It is one of many alternatives to fossil fuels. Mechanical and electrical power can be extracted from wind with the help of wind turbines. Some mechanical applications are water pumping, propelling ships etc. Wind power also has less problematic effects on the environment and has practically zero greenhouse gas emissions.

Many low-power wind turbines built to-date were constructed according to the "Danish concept" , in which wind energy is transformed into electrical energy using a simple squirrel-cage induction machine directly connected to a three-phase power grid. The rotor of the wind turbine is coupled to the generator shaft with a fixed-ratio gearbox. Some induction generators use pole-adjustable winding configurations to enable 26 operation at different synchronous speeds. However, at any given operating point, this Danish turbine basically has to operate at constant speed.

The construction and performance of fixed-speed wind turbines very much depends on the characteristics of mechanical sub circuits, e.g., pitch control time constants, main breaker maximum switching rate, etc. The response time of some of these mechanical circuits may be in the range of tens of milliseconds. As a result, each time a gust of wind hits the turbine, a fast and strong variation of electrical output power can be observed.

These load variations not only require a stiff power grid to enable stable operation, but also require a sturdy mechanical design to absorb high mechanical stresses. This strategy leads to expensive mechanical construction, especially at high-rated power [5].

1.2 Types of wind generators

Until the mid-1990s, most of the installed wind turbines were fixed speed ones, based on squirrel cage induction machines directly connected to the grid, and the generation was always done at constant speed. Today, most of the installed wind turbines are variable speed ones, based on a doubly fed induction generator (DFIG), sharing the market with the wound rotor synchronous generators (WRSGs) and the new arrivals, based on the permanent magnet synchronous generators (PMSGs). All of these generator choices allow variable speed generation [1].

Doubly Fed Induction Generator Solutions:
The doubly fed induction generator has been used for years for variable speed drives. The stator is connected directly to the grid and the rotor is fed by a bidirectional converter that is also connected to the grid. Using vector control techniques, the bidirectional converter assures energy generation at nominal grid frequency and nominal grid voltage independently of the rotor speed. The converter's main aim is to compensate for the difference between the speed of the rotor and the synchronous speed with the slip control.

Full Converter Geared Solutions:
The full converter with gearbox configuration is used with a permanent magnet synchronous generator (PMSG) and squirrel cage induction generator (SCIG). Using vector control techniques again, a bidirectional converter assures energy generation at nominal grid frequency and nominal grid voltage independently of the rotor speed. The SCIG uses a three-stage gearbox to connect the low speed shaft to the high speed shaft. Although today the PMSG machine also uses a two-stage gearbox, the objective is to decrease the gearbox from two stages to one, since the nominal speed of the machine is medium.

Full Converter Direct Drive Solutions:
Two solutions are proposed in the market namely 1) Multipole permanent magnet generator (MPMG) and 2) Multipole wound rotor synchronous generator (WRSG). The multipole permanent magnet generator allows connecting the axis of the machine directly to the rotor of the wind turbine. Using vector control techniques, a bidirectional converter assures energy generation at nominal grid frequency and nominal grid voltage independently of the rotor speed. The biggest disadvantage of this technique is the size of the bidirectional converter, which must be of the same power level as the alternator. Also, the harmonic distortion generated by the converter must be eliminated by a nominal power filter system. The advantage of this technique is the elimination of the mechanical converter (gearbox coupling) because the machine can operate at low speed. Another disadvantage is that the multipole machine requires an elevated number of poles, with the size of the machine being bigger than the generators with the gearbox coupling [1].

1.3 Motivation and Objectives

Wind energy being a renewable, clean resource definitely is one of areas of concern and an area for researchers to develop better innovative solutions in order to tap the power. The motivation behind the project is ability to explain DFIG that is used in wind mills by Electric Machines theory, simple power electronics and control theory. The objectives are to explain the theory involved and models of various parts of DFIG and study behavior of DFIG through its simulation.

1.4 Report Organization

Chapter-1 gives a general introduction to wind power as to how it is a renewable resource, how it is plentiful etc. Then it talks about various types of wind generators used to extract wind power. Then the motivation behind the project and its objectives is talked about.

Chapter-2 develops equations and models of various blocks within DFIG so that DFIG as a whole can be simulated. Firstly, Back-to-Back converter is studied, paying particular attention to the grid side rather than to the rotor side. Not only is the converter itself studied but also its closely associated elements such as the filters, DC link and also its control. The modulation scheme employed (sinusoidal pulse width modulation) to send signals to semi-conductor switches is studied. The grid-side converter control is achieved by GVOVC strategy that involves usage of voltage and current regulators. Then, different dynamic models of the DFIM are developed based on the space vector theory and matrix equations are developed based on these models for simulation purpose. Lastly, DPC control strategy is studied. DPC controls the stator active and reactive powers, achieving reasonably good control performances by injecting appropriate rotor voltage vectors for calculated times.

Chapter-3 mainly deals with the results of the simulation. The effectiveness of a control system can be judged by giving disturbances to the system. On the same line, by giving appropriate disturbances and recording graphs of certain system variables from the simulation, the efficacy of the control systems used in DFIG has been tested. This chapter shows various simulation graphs of a 2MW DFIG, under certain disturbances. Using these transient graphs, the performance of the control systems in the DFIG namely DPC in the rotor side and GVOVC in the stator side are tested for their effectiveness.

Chapter-4 presents the conclusion of the project and also the scope for future work.

CHAPTER-2 ANALYSIS AND MODELING OF DFIG

2.1 Brief Introduction

Before going into analysis of DFIG and its control mechanism, this chapter initially discusses about the back-to-back converter. Along with the converter itself, its grid side control is studied and also other elements of DFIG with which it directly interacts like DC link and filters.

A system can be represented by two models, a steady state model and a dynamic model. A steady state model describes the system attributes after it reaches a state which has many properties unchanging with time. A dynamic model on the other hand covers the behavior of system attributes at all points of time, hence explaining how a system reaches a steady state also, and how a system behaves traversing from one steady state to another. Based on space vector theory, different dynamic models are developed in this chapter. Thus various variables of machine, like current, voltages, fluxes, power, and torque can be continuously evaluated. These models are dictated by differential equations, which can be simulated to study the system.

Lastly, DPC control strategy is studied. DPC controls the stator active and reactive powers, giving moderately good control performances. Rotor side control is carried out in DPC scheme.

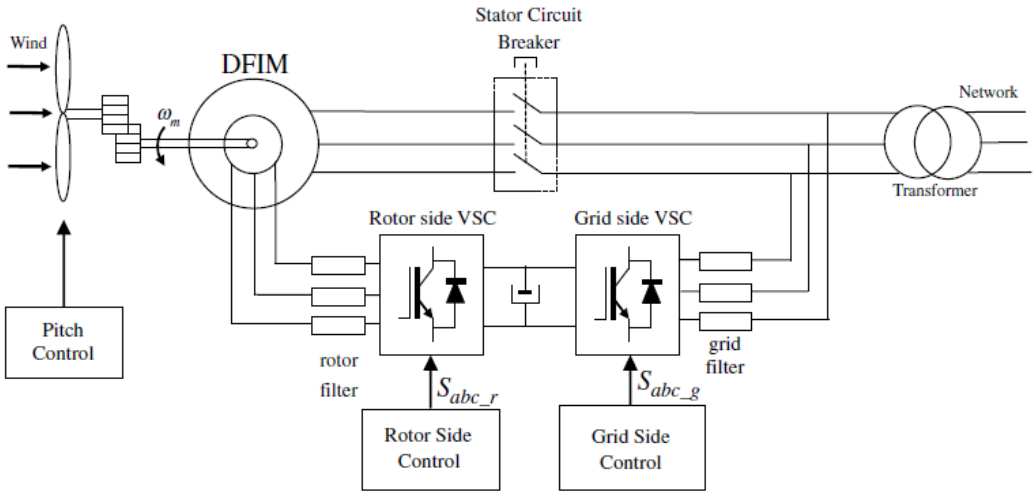

Fig 2.1: Various sections of DFIG based wind turbine [1]

2.2 Voltage Source Converter System (2-level) and Grid-side control

As shown in the Figure 2.1, the bi-directional VSC of DFIG entails a rotor-side convertor, DC link bus and a grid-side convertor. This section explains these aspects including the modulation used in the converters. Only the grid-side convertor is explained, the implementation of rotor-side convertor is more or less the same and hence the important differences are only highlighted. This is followed by explanation of the grid-side control of DFIM.

2.2.1 Grid Side System

The grid side system is composed by the grid side converter, the grid side filter, and the grid voltage. Figure 2.2 illustrates a simplified model of the grid side system.

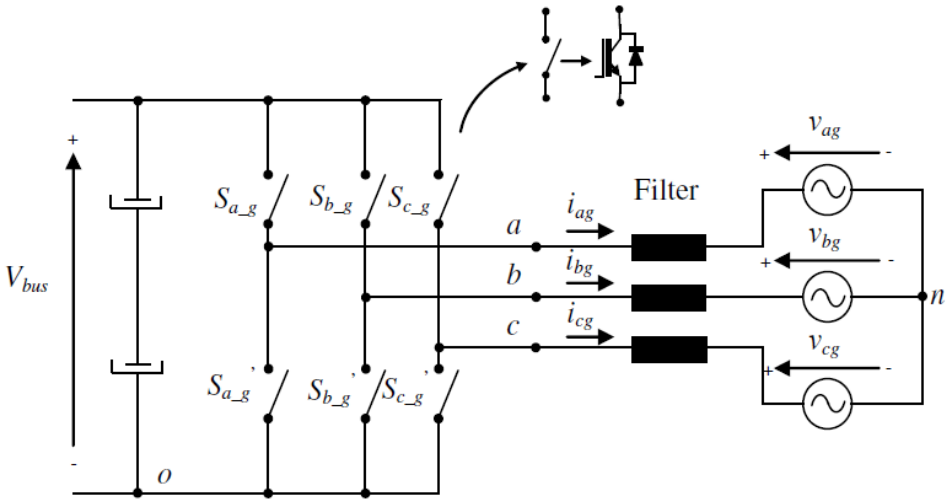

Fig 2.2: Converter, grid-filter, grid-system model [1]

The convertor is designed in such a way that the following protocols holds:

$$S'_{a\_g} = \overline{S_{a\_g}} \tag{2.1}$$

$$S'_{b\_g} = \overline{S_{b\_g}} \tag{2.2}$$

$$S'_{c\_g} = \overline{S_{c\_g}} \tag{2.3}$$

These imply the following equations:

$$v_{ao} = S_{a\_g} V_{bus} \tag{2.4}$$

$$v_{bo} = S_{b\_g} V_{bus} \tag{2.5}$$

$$v_{co} = S_{c\_g} V_{bus} \tag{2.6}$$

But the voltages are with respect to 'o' point of the DC bus. But for modeling reasons, the converter voltages are studies with respect to neutral point of three-phase grid system, 'n' as shown in Figure 2.3.

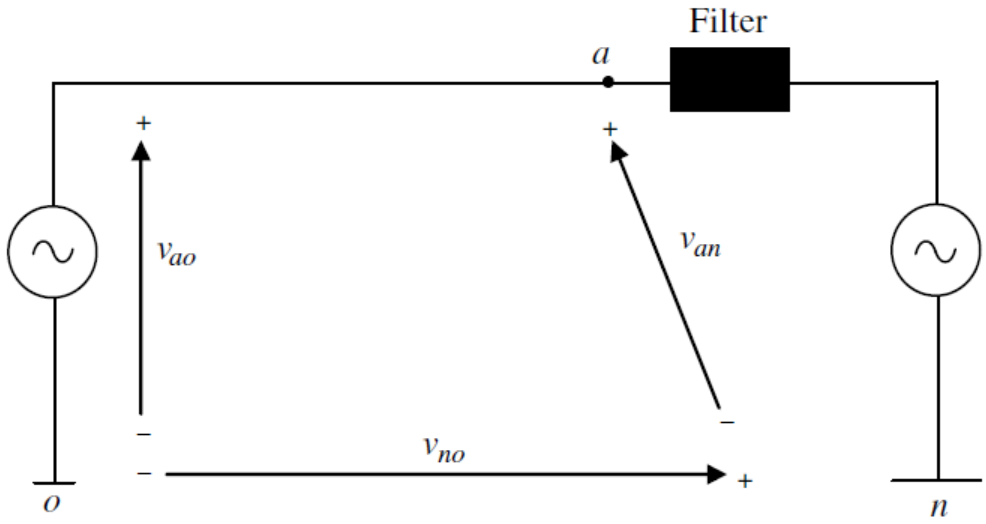

Fig 2.3: Grid-converter, grid-filter, grid-system model [1]

Now assuming a stable grid existing,

$$v_{an} + v_{bn} + v_{bn} = 0 \tag{2.7}$$

$$v_{xn} = v_{xo} - v_{no} \tag{2.8}$$

[Where 'x' collectively represents a, b and c]

On solving them,

$$v_{an} = \frac{V_{bus}}{3}\left(2S_{a\_g} - S_{b\_g} - S_{c\_g}\right) \tag{2.9}$$

$$v_{bn} = \frac{V_{bus}}{3}\left(2S_{b\_g} - S_{a\_g} - S_{c\_g}\right) \tag{2.10}$$

$$v_{cn} = \frac{V_{bus}}{3}\left(2S_{c\_g} - S_{a\_g} - S_{b\_g}\right) \tag{2.11}$$

The signals to trigger the controlled semiconductors of the two-level converter, ON or OFF can be generated according to various modulation schemes. For this project, sinusoidal pulse width modulation (PWM) is employed. The block diagram is shown below in Figure 2.4.

$$S_x = 1 \; if \; v_j^* > v_{tri} \; where \; x = a, b, c \tag{2.12}$$

$$S_x = 0 \; otherwise$$

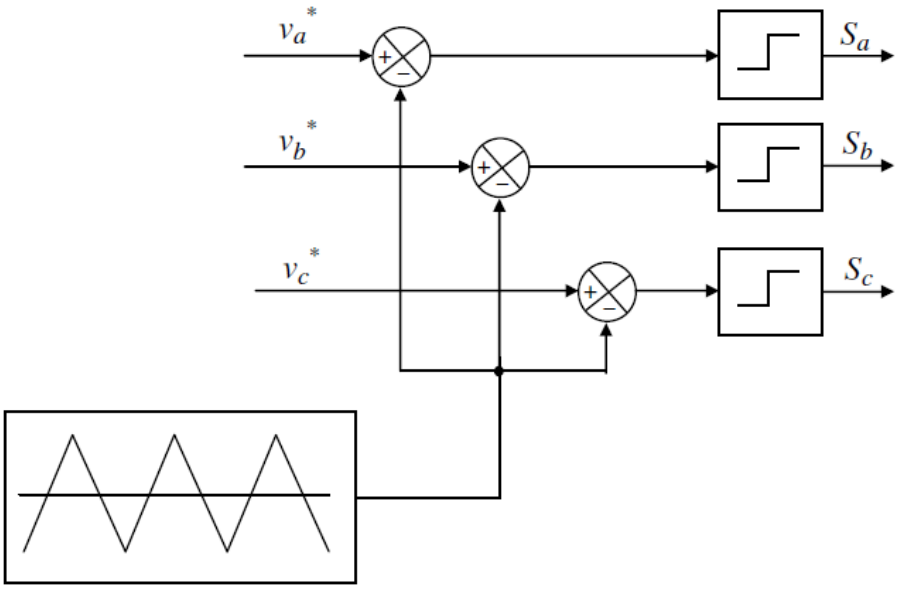

Fig 2.4: Sinusoidal pulse width modulation simulation diagram [1]

Now the converter, inductive filter and the grid combination is modeled by writing equations and developing a block diagram. Fig 2.5 depicts the electrical model. This model applies for all the phases.

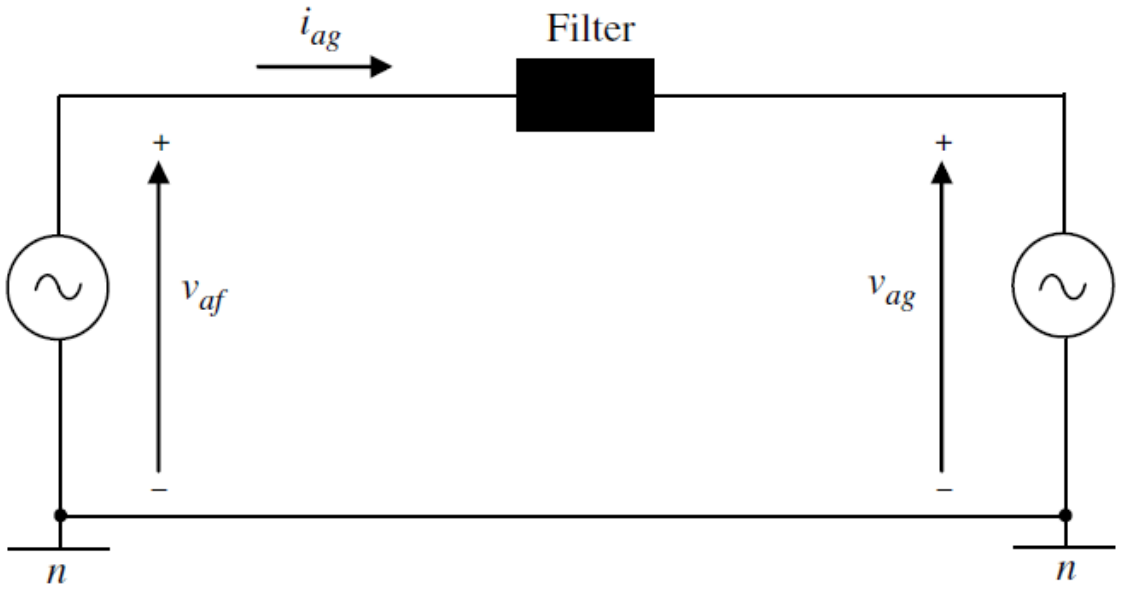

Fig 2.5: Grid-converter, grid-filter, grid-system model [1]

$$v_{af} = R_f i_{ag} + L_f \frac{di_{ag}}{dt} + v_{ag} \tag{2.13}$$

$$v_{bf} = R_f i_{bg} + L_f \frac{di_{bg}}{dt} + v_{bg} \tag{2.14}$$

$$v_{cf} = R_f i_{cg} + L_f \frac{di_{cg}}{dt} + v_{cg} \tag{2.15}$$

2.2.2 Rotor Side System

The implementation of rotor side system is the same as grid side system except for the $\frac{dv}{dt}$ filter involved as shown in Figure 2.6. The $\frac{dv}{dt}$ filter is present to attenuate the step voltages in the rotor terminals of the machine, coming from the converter. This is not necessary from simulation point of view and hence not discussed.

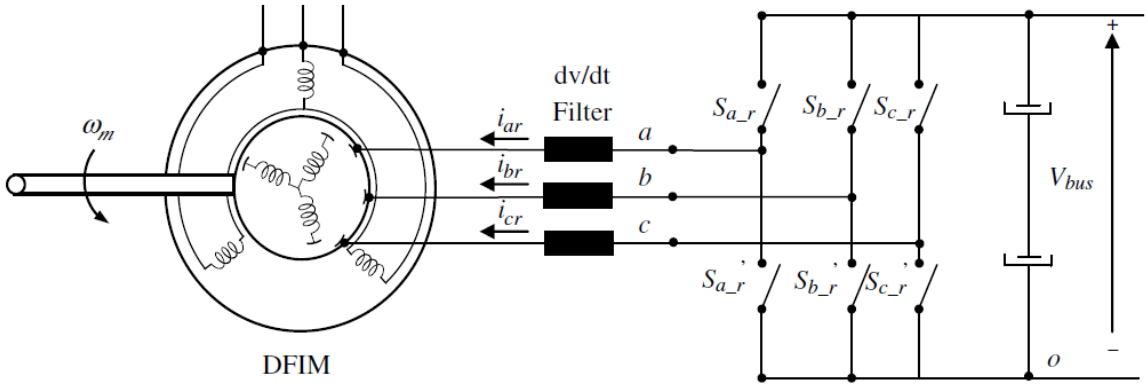

Fig 2.6: Rotor-side converter, rotor-filter, DFIM model [1]

2.2.3 DC link

The DC part of the back-to-back converter is the linkage between the grid side and rotor side converters. This is realized by making use of the fact that the energy stored in a capacitor (or combination of several capacitors), tries to maintain a constant voltage in its terminals. Figure 2.7 shows a possible simplified model of a DC link. It is composed of a capacitor in parallel with a high resistance.

$$V_{bus} = \frac{1}{C_{bus}} \int i_c dt \tag{2.16}$$

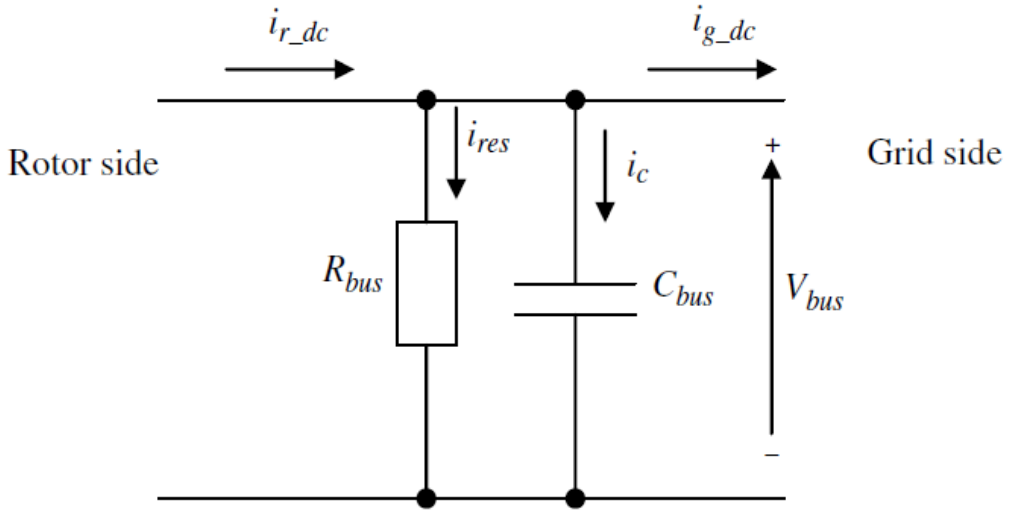

Fig 2.7: DC link system [1]

$$i_c = i_{r\_dc} - i_{g\_dc} - i_{res} \tag{2.17}$$

Now i_{g_dc} and i_{r_dc} can be found out from the grid side converter model developed.

$$i_{g\_dc} = S_{a\_g} i_{ag} - S_{b\_g} i_{bg} - S_{c\_g} i_{cg} \tag{2.18}$$

$$i_{r\_dc} = S_{a\_r} i_{ar} - S_{b\_r} i_{br} - S_{c\_r} i_{cr} \tag{2.19}$$

Thus the following block diagram is developed for simulation purpose:

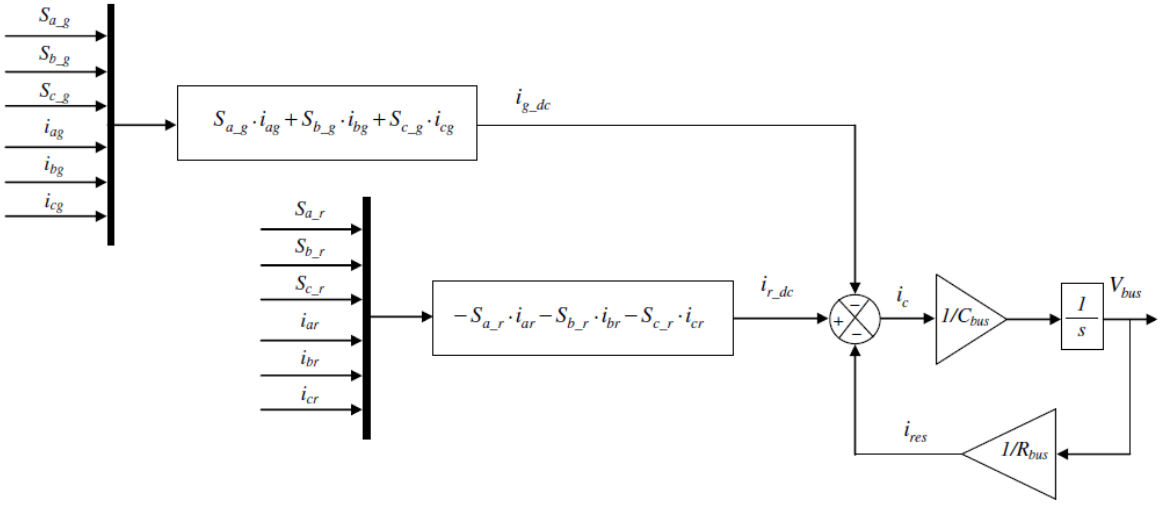

Fig 2.8: DC link system simulation diagram [1]

2.2.4 Control of Grid-side system

The equations (2.13), (2.14) and (2.15) representing the behavior of grid-side converter, grid side filter and the grid transform into the following equations in dq and αβ representation after applying space vector theory.

$$v_{df} = R_f i_{dg} + L_f \frac{di_{dg}}{dt} + v_{dg} - \omega_a L_f i_{qg} \tag{2.20}$$

$$v_{qf} = R_f i_{qg} + L_f \frac{di_{qg}}{dt} + v_{qg} + \omega_a L_f i_{dg} \tag{2.21}$$

$$v_{\alpha f} = R_f i_{\alpha g} + L_f \frac{di_{\alpha g}}{dt} + v_{\alpha g} \tag{2.22}$$

$$v_{\beta f} = R_f i_{\beta g} + L_f \frac{di_{\beta g}}{dt} + v_{\beta g} \tag{2.23}$$

For control purposes, the angular speed of grid voltage ω_s is chosen as synchronous angular speed ω_a and d-axis of the rotating frame is aligned with grid voltage space vector $\vec{v_g^a}$.

$$v_{dg} = |\vec{v_g^a}| \tag{2.24}$$

$$v_{qg} = 0 \tag{2.25}$$

$$\omega_a = \omega_s \tag{2.26}$$

Then the dq frame transform into following equations:

$$v_{df} = R_f i_{dg} + L_f \frac{di_{dg}}{dt} + v_{dg} - \omega_s L_f i_{qg} \tag{2.27}$$

$$v_{qf} = R_f i_{qg} + L_f \frac{di_{qg}}{dt} + L_f i_{dg} \tag{2.28}$$

$$P_g = \frac{3}{2} Re\{\vec{v_g}.\vec{i_g^*}\} = \frac{3}{2}\left(v_{dg} i_{dg} + v_{qg} i_{qg}\right) = \frac{3}{2}|\vec{v_g^a}| i_{dg} \tag{2.29}$$

$$Q_g = \frac{3}{2} Im\{\vec{v_g}.\vec{i_g^*}\} = \frac{3}{2}\left(v_{dg} i_{dg} - v_{qg} i_{qg}\right) = -\frac{3}{2}|\vec{v_g^a}| i_{qg} \tag{2.30}$$

$$P_f = \frac{3}{2} Re\{\vec{v_f} . \vec{i_g^*}\} = \frac{3}{2}\left(v_{df} i_{dg} + v_{qf} i_{qg}\right) = \frac{3}{2}\left(R_f |\vec{i_g}|^2 + v_{dg} i_{dg}\right) \quad (2.31)$$

$$Q_f = \frac{3}{2} Im\{\vec{v_f} . \vec{i_g^*}\} = \frac{3}{2}\left(v_{qf} i_{dg} - v_{df} i_{qg}\right) = \frac{3}{2}\left(L_f \omega_s |\vec{i_g}|^2 - v_{dg} i_{dg}\right) \quad (2.32)$$

Based on the above equations a control system namely Grid voltage vector oriented vector control (GVOVC) is devised. The block diagram of which is described in the Figure 2.9 below.

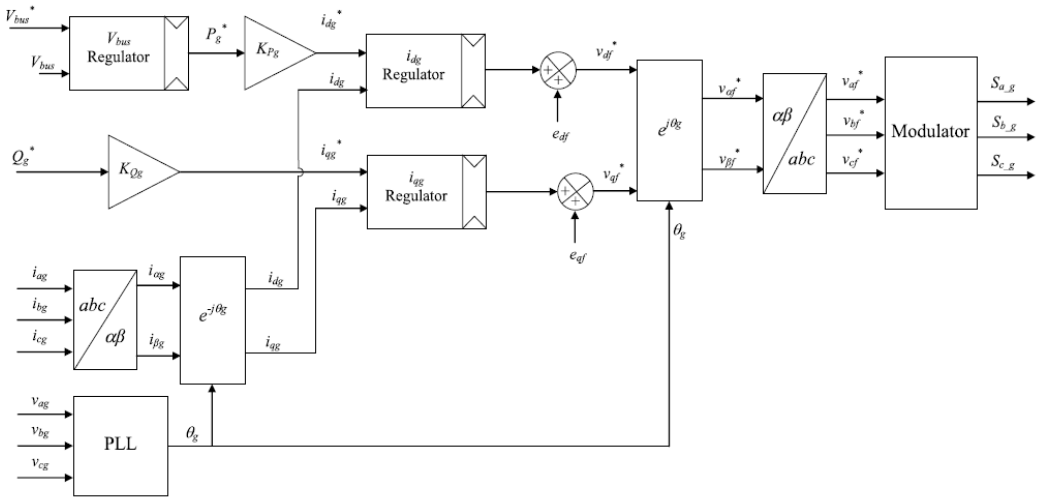

Fig 2.9: GVOVC simulation diagram [1]

$$e_{df} = -\omega_s L_f i_{qg} \quad e_{qf} = \omega_s L_f i_{dg} \quad (2.33)$$

$$K_{Pg} = \frac{1}{\frac{3}{2} v_{dg}} \qquad K_{Pg} = \frac{1}{-\frac{3}{2} v_{dg}} \quad (2.34)$$

The PLL structure block is explained in the Figure 2.10:

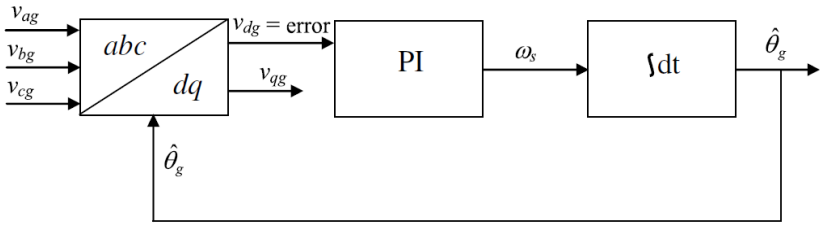

Fig 2.10: PLL simulation diagram [1]

2.3 Dynamic Modeling of the Doubly Fed Induction machine

The DFIM can be described as three windings in the rotor and three stator windings as shown in Figure 2.11.

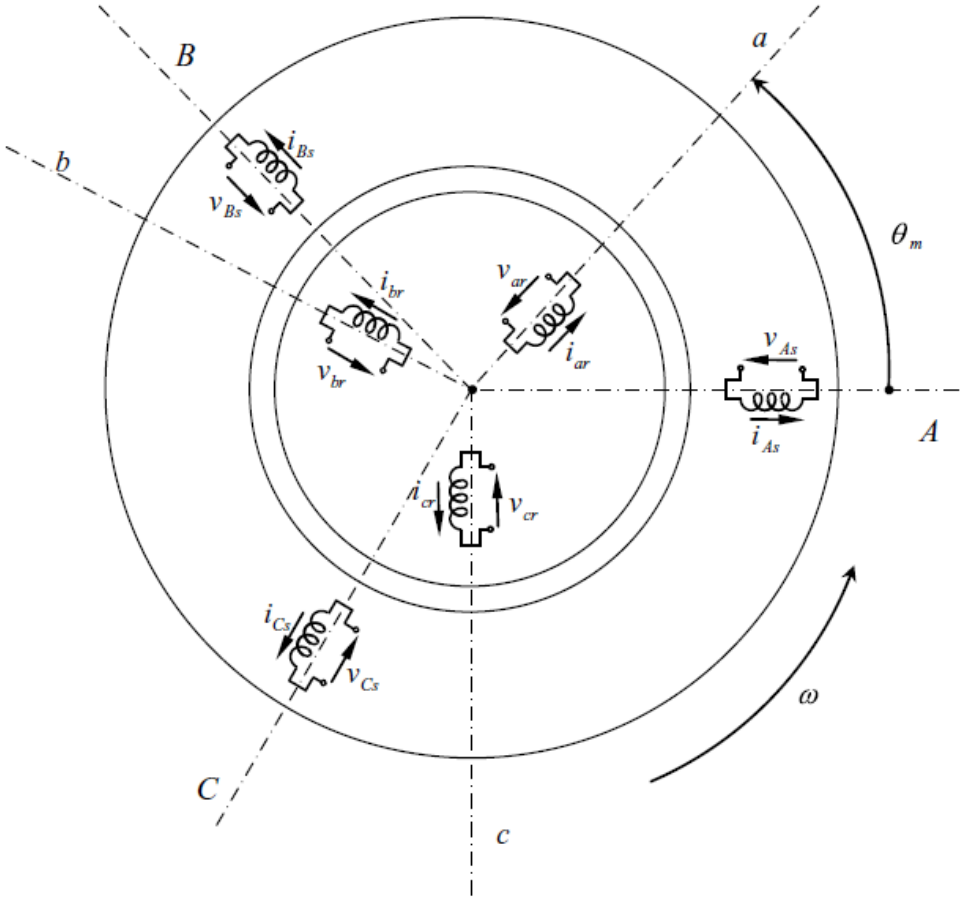

Fig 2.11: Ideal three phase windings of DFIM [1]

$$v_{as}(t) = R_s i_{as}(t) + \frac{d\psi_{as}(t)}{dt} \tag{2.35}$$

$$v_{bs}(t) = R_s i_{bs}(t) + \frac{d\psi_{bs}(t)}{dt} \tag{2.36}$$

$$v_{cs}(t) = R_s i_{cs}(t) + \frac{d\psi_{cs}(t)}{dt} \tag{2.37}$$

$$v_{ar}(t) = R_r i_{ar}(t) + \frac{d\psi_{ar}(t)}{dt} \tag{2.38}$$

$$v_{br}(t) = R_r i_{br}(t) + \frac{d\psi_{br}(t)}{dt} \tag{2.39}$$

$$v_{cr}(t) = R_r i_{cr}(t) + \frac{d\psi_{cr}(t)}{dt} \tag{2.40}$$

$$\omega_m = \omega_s - \omega_r \tag{2.41}$$

$$\omega_m = \frac{p}{2}\Omega_m \tag{2.42}$$

$$s = \frac{\omega_s - \omega_m}{\omega_s} \tag{2.43}$$

Using the space vector theory the above equations, i.e, the voltage and flux equations can be written as follows:

$$\vec{v_s^s} = R_s \vec{i_s^s} + \frac{d\vec{\psi_s^s}}{dt} \tag{2.44}$$

$$\vec{v_r^r} = R_r \vec{i_r^r} + \frac{d\vec{\psi_r^r}}{dt} \tag{2.45}$$

$$\vec{\psi_s^s} = L_s \vec{i_s^s} + L_m \vec{i_r^s} \tag{2.46}$$

$$\vec{\psi_r^r} = L_m \vec{i_s^r} + L_r \vec{i_r^r} \tag{2.47}$$

$$L_s = L_{\sigma s} + L_m \tag{2.48}$$

$$L_r = L_{\sigma r} + L_m \tag{2.49}$$

Using the above equations, DFIM can be studies in αβ or dq or DQ coordinates using space vector approach. They can be transformed from one form to another using their angular speeds and their difference in angular position. The αβ and dq model of DFIM have been depicted in the figures that follow. The αβ model (Figure 2.12) analyzes the system with

respect to stator while the dq model (Figure 2.13) analyzes the system with respect to synchronous speed of DFIM.

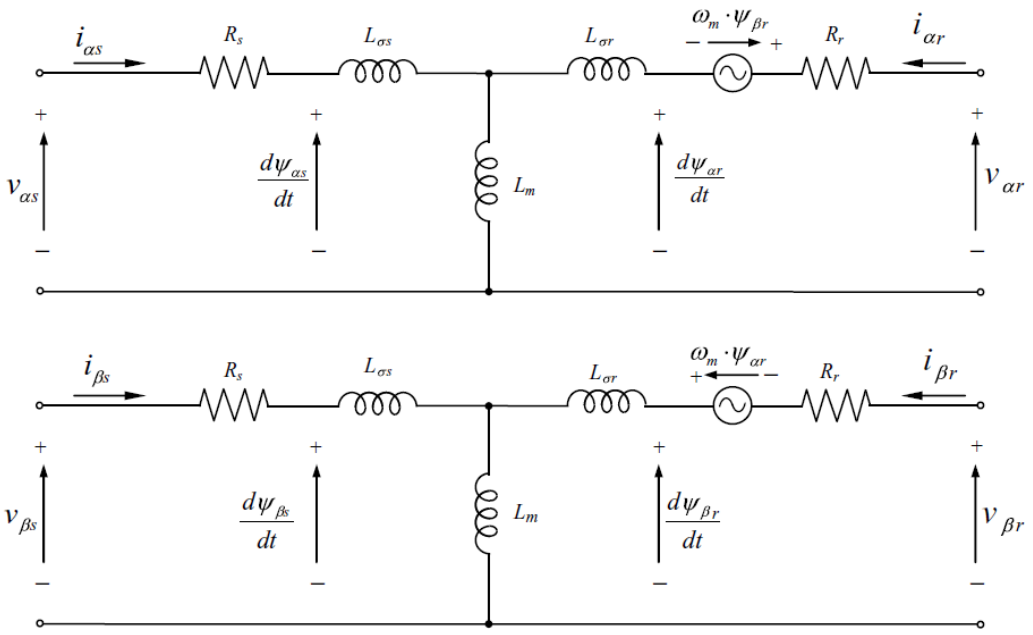

Fig 2.12: $\alpha\beta$ model of DFIM (i.e, stator reference frame) [1]

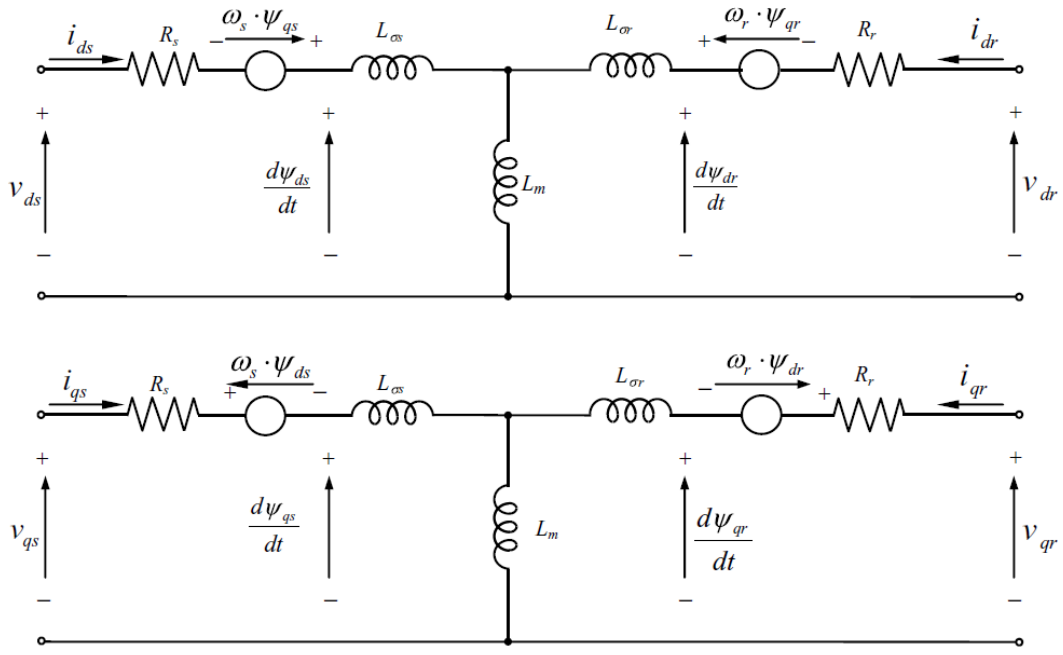

Fig 2.13: dq model of DFIM (i.e, rotor reference frame) [1]

$$P_s = \frac{3}{2} Re\{\vec{v_s}.\vec{i_s^*}\} = \frac{3}{2}\left(v_{\alpha s} i_{\alpha s} + v_{\beta s} i_{\beta s}\right) \tag{2.50}$$

Similarly, P_r or Q_s or Q_r can be calculated on same lines even in dq frame. Now for the electromagnetic torque,

$$T_{em} = \tfrac{3}{4} pIm\{\vec{\psi_r}.\vec{i_r^*}\} = \tfrac{3}{4} p\left(\psi_{\beta r} i_{\alpha r} - \psi_{\alpha r} i_{\beta r}\right) \tag{2.51}$$

Considering fluxes as state space magnitudes, the following equations are obtained:

$$\frac{d\begin{bmatrix}\Psi_s^{\rightarrow s}\\ \Psi_r^{\rightarrow s}\end{bmatrix}}{dt} = \begin{bmatrix} -\frac{R_s}{\sigma L_s} & \frac{R_s L_m}{\sigma L_s L_r} \\ \frac{R_r L_m}{\sigma L_s L_r} & -\frac{R_r}{\sigma L_r} + j\omega_m \end{bmatrix}\begin{bmatrix}\Psi_s^{\rightarrow s}\\ \Psi_r^{\rightarrow s}\end{bmatrix} + \begin{bmatrix}\mathrm{v}_s^{\rightarrow s}\\ \mathrm{v}_r^{\rightarrow s}\end{bmatrix} \tag{2.52}$$

$$\frac{d\begin{bmatrix}\psi_{\alpha s}\\ \psi_{\beta s}\\ \psi_{\alpha r}\\ \psi_{\beta r}\end{bmatrix}}{dt} = \begin{bmatrix} -\frac{R_s}{\sigma L_s} & 0 & \frac{R_s L_m}{\sigma L_s L_r} & 0 \\ 0 & -\frac{R_s}{\sigma L_s} & 0 & \frac{R_s L_m}{\sigma L_s L_r} \\ \frac{R_r L_m}{\sigma L_s L_r} & 0 & -\frac{R_r}{\sigma L_r} & -\omega_m \\ 0 & \frac{R_r L_m}{\sigma L_s L_r} & \omega_m & -\frac{R_r}{\sigma L_r} \end{bmatrix}\begin{bmatrix}\psi_{\alpha s}\\ \psi_{\beta s}\\ \psi_{\alpha r}\\ \psi_{\beta r}\end{bmatrix} + \begin{bmatrix}v_{\alpha s}\\ v_{\beta s}\\ v_{\alpha r}\\ v_{\beta r}\end{bmatrix} \tag{2.53}$$

Now, considering fluxes as state space magnitudes, the following equations are obtained:

$$\frac{d\begin{bmatrix}i_s^{\rightarrow s}\\ i_r^{\rightarrow s}\end{bmatrix}}{dt} = \left(\frac{1}{\sigma L_s L_r}\right)\begin{bmatrix} -R_s L_r - j\omega_m {L_m}^2 & R_r L_m - j\omega_m L_m L_r \\ R_s L_m + j\omega_m L_s L_m & -R_r L_s + j\omega_m L_s L_r \end{bmatrix}\begin{bmatrix}i_s^{\rightarrow s}\\ i_r^{\rightarrow s}\end{bmatrix} + \left(\frac{1}{\sigma L_s L_r}\right)\begin{bmatrix} L_r & -L_m \\ -L_m & L_s \end{bmatrix}\begin{bmatrix}v_s^{\rightarrow s}\\ v_r^{\rightarrow s}\end{bmatrix} \tag{2.54}$$

$$\frac{d\begin{bmatrix} i_{\alpha s} \\ i_{\beta s} \\ i_{\alpha r} \\ i_{\beta r} \end{bmatrix}}{dt} = \left(\frac{1}{\sigma L_s L_r}\right)\begin{bmatrix} -R_s L_r & \omega_m {L_m}^2 & R_r L_m & \omega_m L_m L_r \\ -\omega_m {L_m}^2 & -R_s L_r & -\omega_m L_m L_r & R_r L_m \\ R_s L_m & -\omega_m L_s L_m & -R_r L_s & -\omega_m L_s L_r \\ \omega_m L_s L_m & R_s L_m & \omega_m L_s L_r & -R_r L_s \end{bmatrix}\begin{bmatrix} i_{\alpha s} \\ i_{\beta s} \\ i_{\alpha r} \\ i_{\beta r} \end{bmatrix} + \left(\frac{1}{\sigma L_s L_r}\right)\begin{bmatrix} L_r & 0 & -L_m & 0 \\ 0 & L_r & 0 & -L_m \\ -L_m & 0 & L_s & 0 \\ 0 & -L_m & 0 & L_s \end{bmatrix}\begin{bmatrix} v_{\alpha s} \\ v_{\beta s} \\ v_{\alpha r} \\ v_{\beta r} \end{bmatrix} \tag{2.55}$$

The matrix equations above are used to develop a simulation diagram for the DFIM as shown in Figure 2.14.

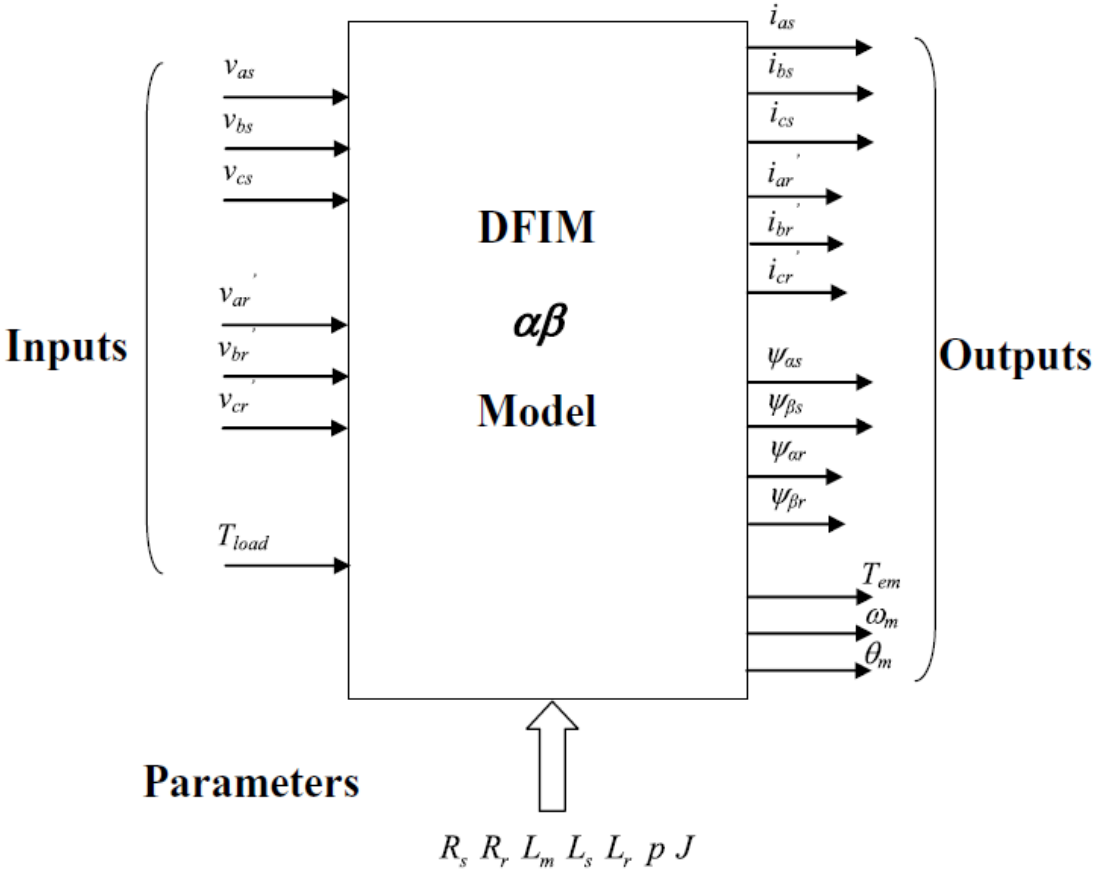

Fig 2.14: Inputs and outputs of DFIM simulation diagram [1]

Equations for all the variables present in the above diagram except for ω_m and θ_m had been derived. These can be calculated by the mechanical equation described below.

$$T_{em} - T_{load} = J\frac{d\Omega_m}{dt} \tag{2.56}$$

2.4 Direct Power Control

DPC strategy used here seeks to control stator active and stator reactive power ultimately through control of rotor voltage. The implementation is explained in this section.

$$\vec{v_r^r} = R_r\vec{i_r^r} + \frac{d\vec{\psi_r^r}}{dt} \tag{2.57}$$

It is safe to drop the first term of RHS of above equation for purpose of simplicity.

$$\vec{v_r^r} \cong \frac{d\vec{\psi_r^r}}{dt} \tag{2.58}$$

$$|\vec{\psi_r^r}|_{final} \cong |\vec{\psi_r^r}|_{initial} + \int_0^t \vec{v_r^r}\,dt \tag{2.59}$$

Assuming a particular voltage vector is inserted for a time h. Then,

$$|\vec{\psi_r^r}|_{final} \cong |\vec{\psi_r^r}|_{initial} + \vec{v_r^r}h \tag{2.60}$$

So by inserting different rotor voltage vectors depending on the angular position of flux vector with respect to DQ (rotor frame) frame, flux changes can be influenced as shown.

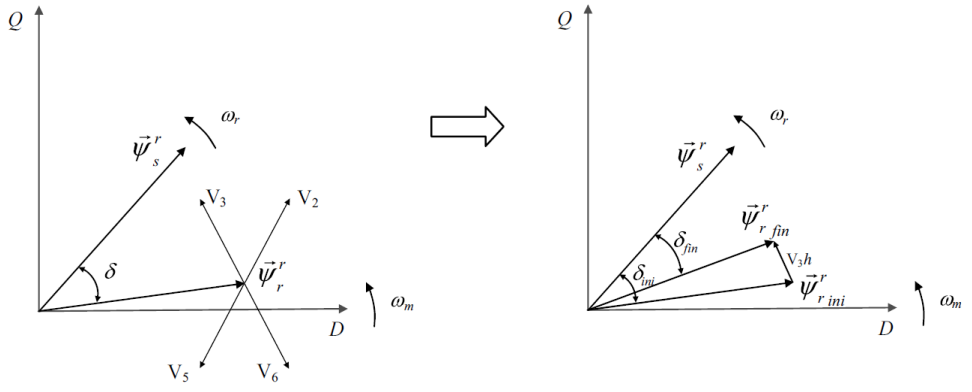

Fig 2.15: Stator and Rotor flux positions [1]

Now this fact is used in control of stator and reactive powers as they depend on the rotor flux vector and relative angle between stator and rotor flux space vectors as shown ahead.

$$P_s = \frac{3}{2} Re\{\vec{v_s} . \vec{i_s}^*\} \tag{2.61}$$

$$Q_s = \frac{3}{2} Im\{\vec{v_s} . \vec{i_s}^*\} \tag{2.62}$$

Using the dynamic model equations developed earlier,

$$P_s = \frac{3}{2} \frac{L_m}{\sigma L_s L_r} \omega_s |\vec{\psi_s}| |\vec{\psi_r}| \sin\delta \tag{2.63}$$

$$Q_s = \frac{3}{2} \frac{\omega_s}{\sigma L_s} |\vec{\psi_s}| \left[\frac{L_m}{L_r} |\vec{\psi_s}| - |\vec{\psi_r}| \cos\delta \right] \tag{2.64}$$

Assuming the stator voltage is fixed, the equations are of the form:

$$P_s = l |\vec{\psi_r}| \sin\delta \tag{2.65}$$

$$Q_s = m[n - |\vec{\psi_r}| \cos\delta] \tag{2.66}$$

[Where l, m and n are constants]

Hence, the stator active and reactive powers can be influenced by maneuvering the rotor voltage by injecting calculated voltage vectors.

With the help of the above equations, and by employing hysteresis controllers, a simulation block for DPC is made in Fig 2.16. Fig 2.17 shows the ON-OFF hysteresis controllers for P_s and Q_s. The appropriate vectors to be injected is decided based on Fig 2.18. This table can easily be worked out based on sector of rotor flux vector, and the outputs of the hysteresis controllers.

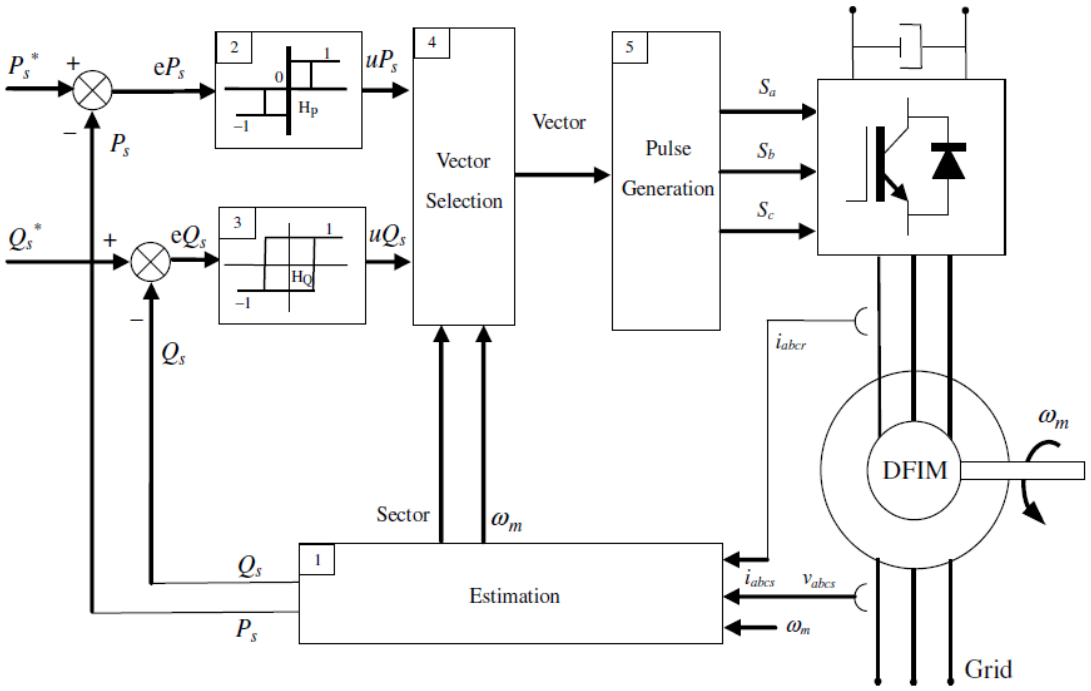

Fig 2.16: Direct Power Control simulation diagram [1]

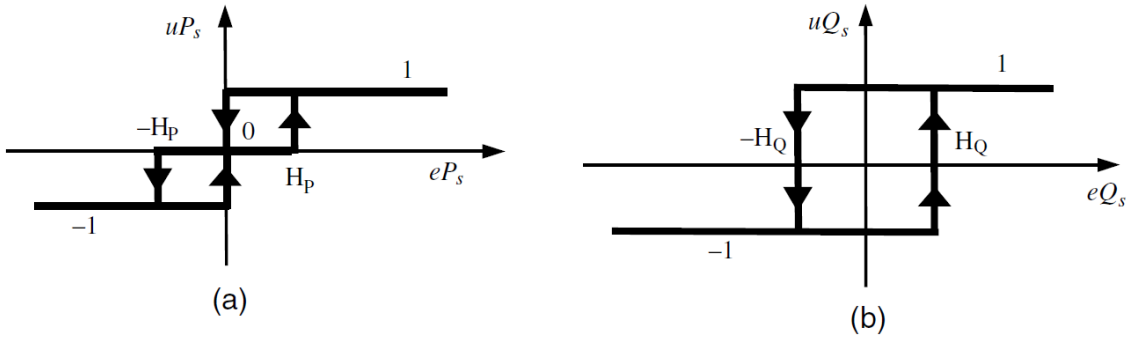

Fig 2.17: ON-OFF P_s and $Q_s$controller with hysteresis band [1]

		uP_s		
		1	0	−1
uQ_s	1	$V_{(k-2)}$	V_0, V_7	$V_{(k+2)}$
	−1	$V_{(k-1)}$	V_0, V_7	$V_{(k+1)}$

Fig 2.18 [k is the sector number]: Vector selection table [1]

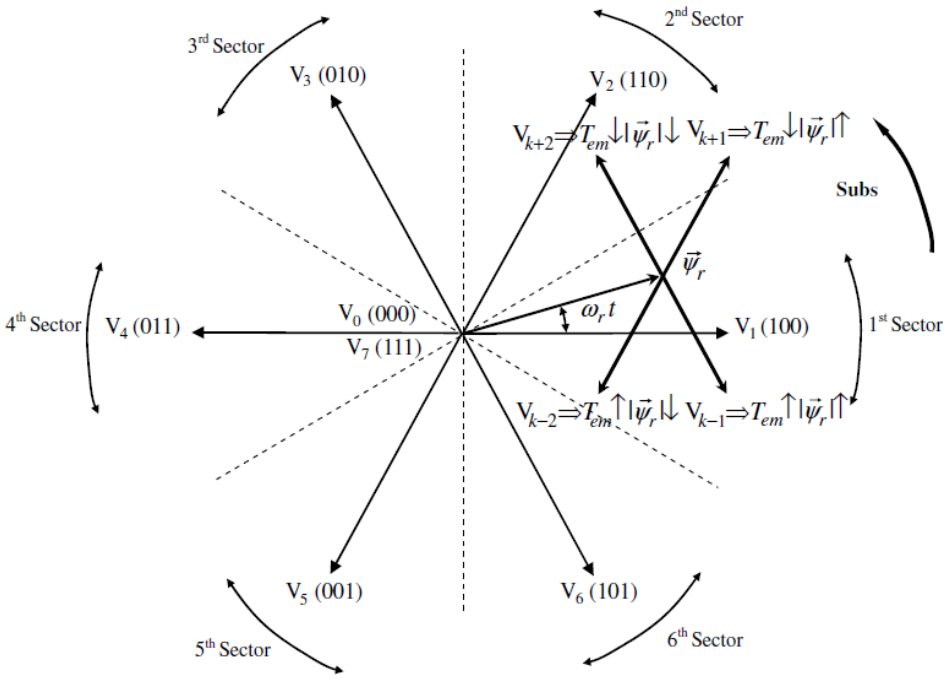

Fig 2.19: Voltage vectors and their effect on the stator active and reactive power at sub-synchronous speed in the motor mode [1]

2.5 Summary

In this chapter, the theory behind DFIG was built and block diagrams were developed from various models and equations to aid in the simulation. Initially, the grid-side converter, grid- side filter and grid-system combination was discussed with help of simple ON-OFF principle of switches, sinusoidal pulse width modulation and a simple electrical model. This was followed by capacitive modeling of DC link present in 2- level converter. The Grid side control was implemented by Grid voltage vector oriented vector control (GVOVC) which involved use of current and voltage regulators and PLL estimation. Then a dynamic model of Doubly fed induction machine was developed using space vector theory. A matrix of equations was developed for the simulation purpose. Lastly, the Direct Power Control was studied wherein by injecting voltage vectors to change rotor voltage; rotor flux space vector and its angle with stator flux space vector can be influenced which in turn influences the stator active and reactive power.

CHAPTER-3 SIMULATION RESULTS AND DISCUSSION

3.1 The system details

A 2MW DFIG is simulated using the theory developed before. The real characteristics and parameters of a common 2MW have been employed for the simulation and are shown in Figure 3.1.

Table showing characteristic values of 2MW DFIG:

Synchronous speed (rev/min)	1500
Rated power (kW)	2000
Rated line-to-line stator voltage (V_{rms})	690
Rated stator current (I_{rms})	1760
Rated torque (Nm)	12732
p	2
Rated V_r (V_{rms}) 2070	2070
u	0.34
R_s (mΩ)	2.6
$L_{\sigma s}$ (mH)	0.087
L_m (mH)	2.5
R'_r (mΩ)	26.1
$L'_{\sigma r}$ (mH)	0.783
R_r (mΩ)	2.9
$L_{\sigma r}$ (mH)	0.087
L_s (mH)	2.587
L_r (mH)	2.587
V_{base}	398.4
I_{base}	1760
r_s	0.011
l_{ss}	0.12
l_m	3.45
r_r	0.012
l_{sr}	0.12

Fig 3.1: 2MW DFIG characteristic values [1]

3.2 Simulation results

The effectiveness of a control system can be judged by giving disturbances to the system. On the same line, by giving appropriate disturbances and recording graphs of certain system variables from the simulation, the efficacy of the control systems used in DFIG has been tested.

Firstly, the DPC from rotor side is being tested. For this $Q_{s_{pu}}$ is made from 0 pu to 0.4 pu. The slip s is -0.25. Negative sign of $P_{s_{pu}}$ implies generating operation. This is shown in Figure 3.2.

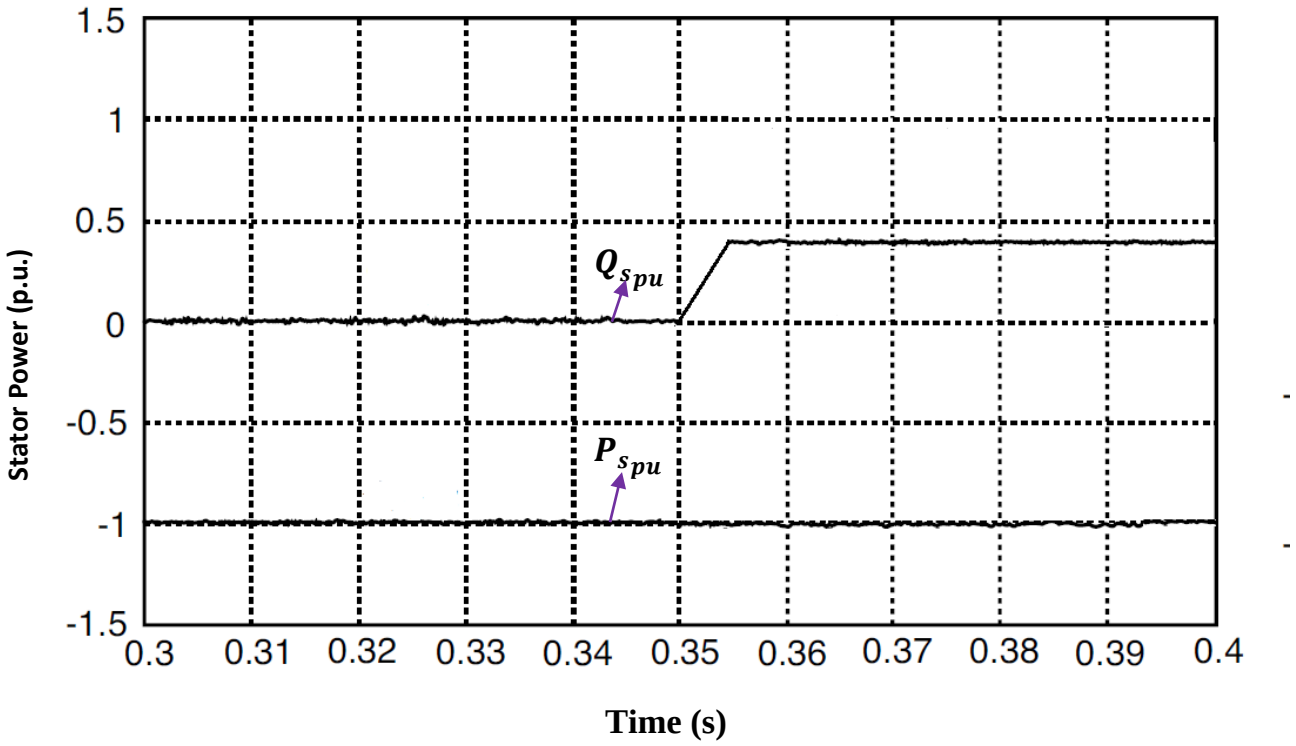

Fig. 3.2: $Q_{s_{pu}}$ and $Q_{s_{pu}}$ plot

The waveforms of stator voltages and stator currents are recorded as shown in Figure 3.3 and Figure 3.4.

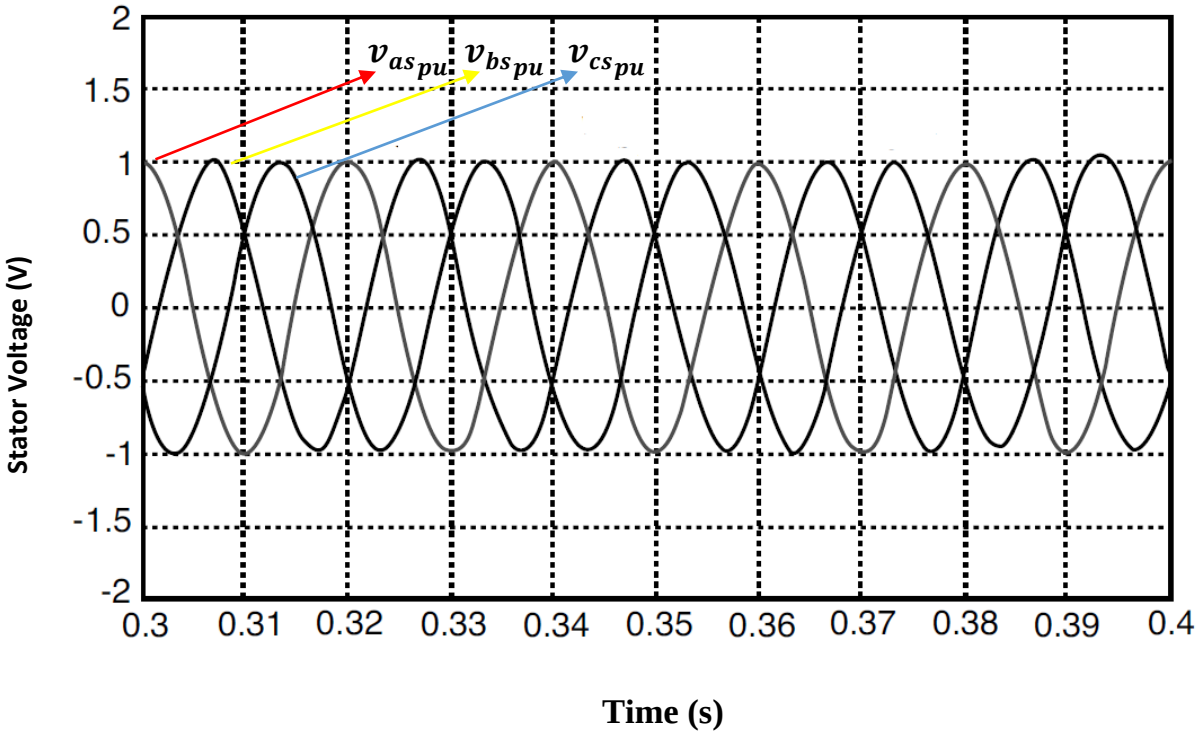

Fig. 3.3: Stator voltages

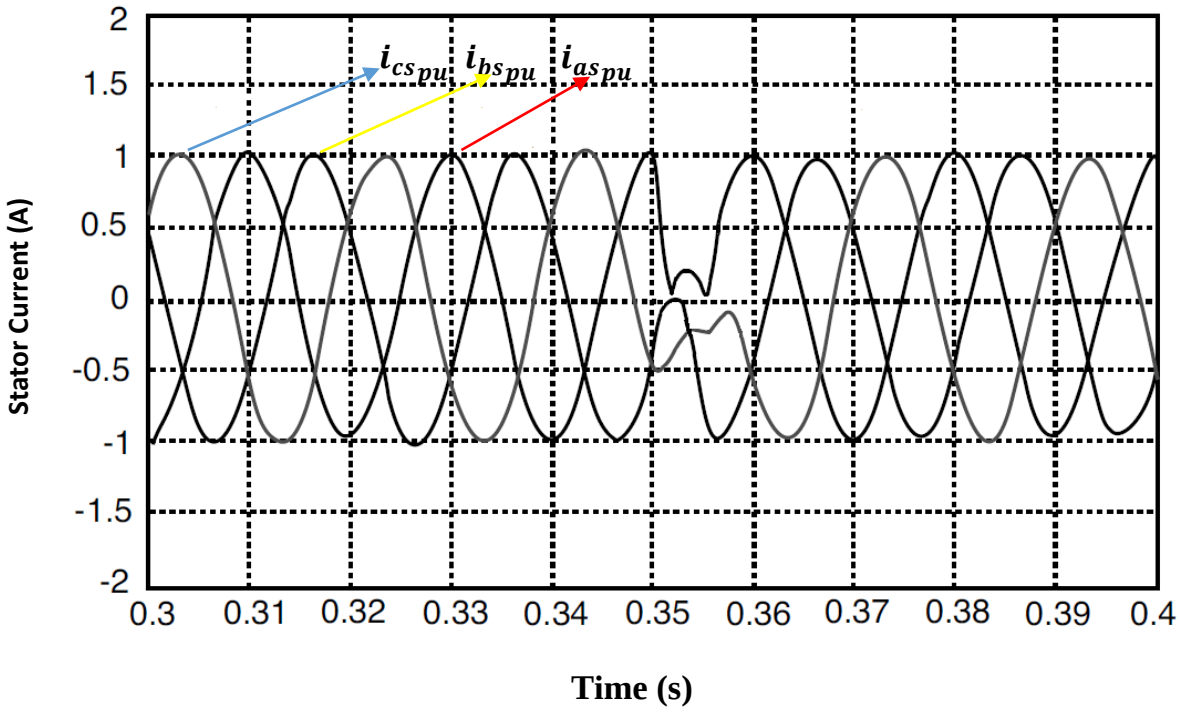

Fig. 3.4: Stator currents

It can be observed from the graphs, particularly during the transient state that the transitions were quite smooth without any overshoots or damping all owing to the proper functioning of the DPC control block.

Now the GVOVC from the grid side is tested. For this, Q_g made from 0 pu to 0.4 pu as shown in the Figure 3.5. It can be inferred from the smooth graphs as given in Figure 3.6 depicting current from converter to grid in dq frame and Figure 3.7 depicting V_{bus} that this control is also performing properly.

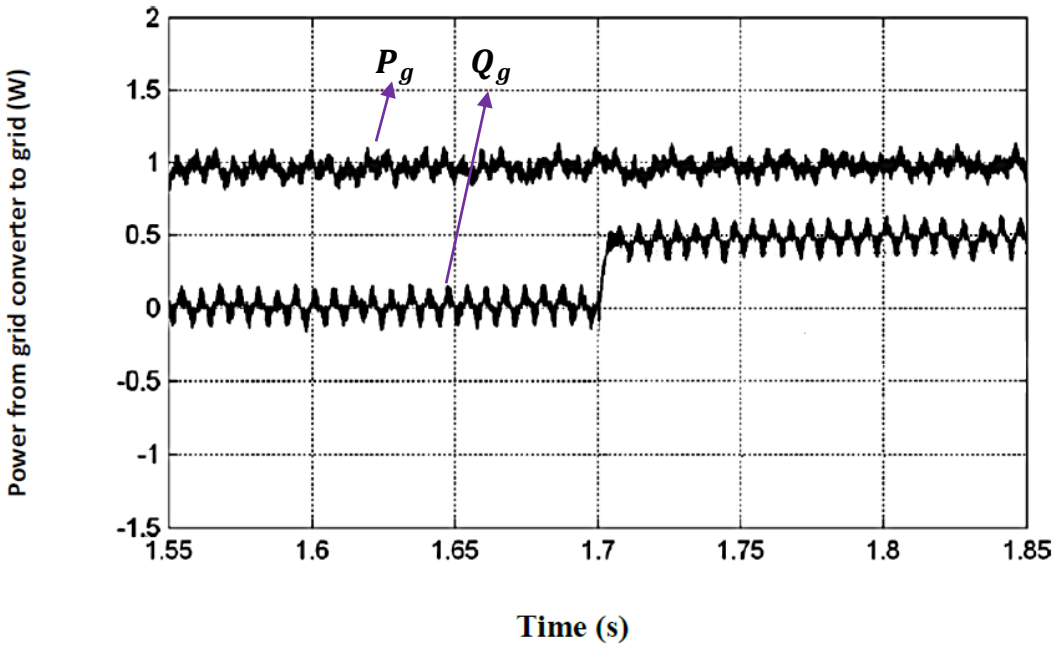

Fig 3.5: P_g and Q_g plot

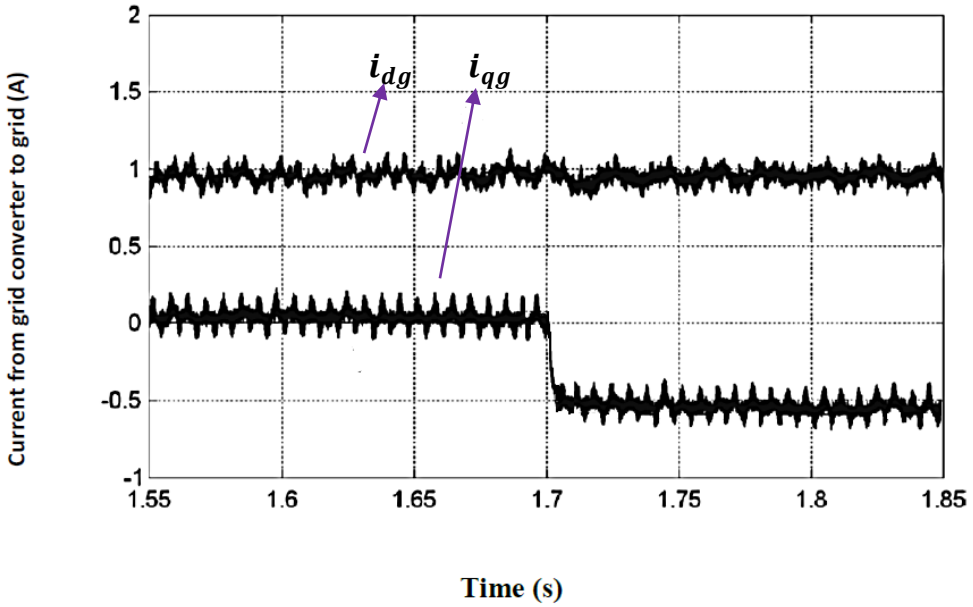

Fig 3.6: i_{dg} and i_{qg} plot

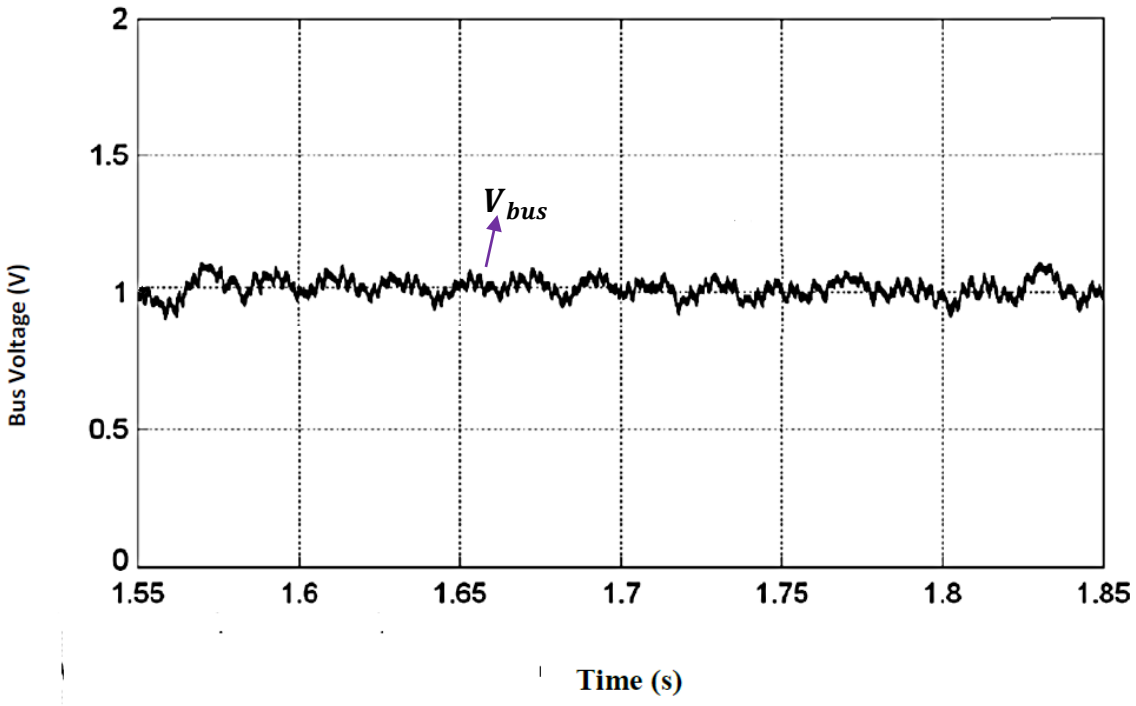

Fig 3.7: V_{bus} plot

3.3 Summary

In this chapter, various simulation graphs of a 2MW DFIG, under certain disturbances were studied. Using these transient graphs, the performance of the control systems in the DFIG namely DPC in the rotor side and GVOVC in the stator side were tested for their efficacy.

CHAPTER-4 CONCLUSION

4.1 Conclusion of the project

The theory behind working of various parts of a DFIG has been explained in this report. Suitable simulation diagrams or matrices were developed for each one of them. Finally, with the help of graphs of different variables obtained from the simulation capturing the transient effects of various disturbances, the effectiveness of the control of the DFIG was studied. Indeed, the role of the control systems could be appreciated by the smooth transition or functioning of various variables without any abrupt shoot ups or fall downs.

4.2 Scope for future work

It is anticipated that, as a result of the wide range of emerging technologies, there will not be a unique gear–generator–converter technology for wind turbines in the near future, and manufacturers will tend to diversify the wind turbine solutions, establishing their own particular solutions, in many cases very close to one another, but probably still combining the direct drive solution with a full scale converter, the geared full scale converter solution, and the geared doubly fed based solution with reduced scale converter.

However, future wind turbine technology must also innovate the mechanical structure of the wind turbine itself, guarantee increasing penetration into the market with efficient and reliable grid integration, widen the location of wind turbines by developing their capabilities (low wind, offshore, etc.), and increase diversification while paying attention to environmental concerns.

Consequently, in order to optimize wind turbine technology in a more efficient and reliable way, it is necessary to coordinate the innovation efforts, yielding a more integrated design. At the same time the application itself must be considered, together with all the elements of the wind turbine: the electric generator, the converter, the gear, the mechanical structure, the aerodynamics, the location, grid integration, and so on [1].

REFERENCES

[1] *Doubly Fed Induction Machine: Modeling and Control for Wind Energy Generation, First Edition*. By G. Abad, J. Lo´pez, M. A. Rodrıguez, L. Marroyo, and G. Iwanski, 2011, The Institute of Electrical and Electronic Engineers, Inc. Published 2011 by JohnWiley&Sons, Inc.

[2] A. Peterson, "Analysis, Modeling and Control of Doubly-Fed Induction Generators for Wind Turbines." *Ph.D. thesis*, Chalmers University of Technology, Goteborg, Sweden, 2005.

[3] Modeling and Control of a Wind Turbine Driven Doubly Fed Induction Generator Arantxa Tapia, Gerardo Tapia, J. Xabier Ostolaza, and José Ramón Sáenz *IEEE Transactions on energy conversion*, Vol. 18, No. 2, pg 194-204, June 2003.

[4] L. Xu and P. Cartwright, "Direct Active and Reactive Power Control of DFIG for Wind Energy Generation," *IEEE Trans. Energy Conversion*, Vol. 21, No. 3, pp. 750–758, September 2006.

[5] Doubly fed induction generation systems for wind turbine, by S. Muller, M. Deicke, & Rik W. De Doncker, *IEEE Industry Applications Magazine*, May-June 2002.